Supplemental Information
Electric Field Induced Macroscopic Cellular Phase of Nanoparticles

Abigail Rendos[+,1] Wenhan Cao[+,2,†] Margaret Chern,[1] Marco Lauricella,[3] Sauro Succi,[3] Jörg G. Werner,[1,2] Allison M. Dennis,[1,4] Keith A. Brown,[1,2,5,*]

[1] Division of Materials Science & Engineering, Boston University, Boston, MA, USA.

[2] Department of Mechanical Engineering, Boston University, Boston, MA, USA.

[3] Center for Life Nano-Neuro Science at La Sapienza, Rome, Italy.

[4] Biomedical Engineering Department, Boston University, Boston, MA, USA.

[5] Physics Department, Boston University, Boston, MA, USA.

[+]Contributed Equally

[†]Present address: School of Information Science and Technology, ShanghaiTech University, Shanghai, China.

*Corresponding Author: Keith A. Brown, email address: brownka@bu.edu

I.   Cahn-Hilliard Analysis

To analyze the spinodal decomposition of the particles from a uniform distribution to a cellular phase, we perform a Cahn-Hilliard analysis. As an initial state for this analysis, we posit that the DC electric field E will lead the particles to assemble onto the electrode that is positively charged. To justify this, we estimate the electrophoretic speed v_p of the quantum dots (QDs) which is given by,[1]

$$v_p = \frac{\varepsilon_m \zeta_p E}{\eta} \text{ for } \kappa R \gg 1, \tag{S1}$$

with particle radius R, inverse Debye length κ, particle zeta potential ζ_p, medium permittivity ε_m, and medium viscosity η. For our system of QDs suspended in 3.125 mM borate buffer, $\kappa = 0.18$ nm^{-1} and $R = 8.5$ nm, so $\kappa R > 1$. Based on Eq. S1, a particle[2] with $\zeta_p \cong -30$ mV at room temperature in water will move ~0.2 mm/s when 2 V is applied across 200 μm. Under these conditions, the particle would traverse the fluid cell in ~1 s, so all the particles will concentrate on the electrode immediately upon application of E. If the QDs have a packing fraction of 0.74 and are dispersed at a bulk volume fraction φ of 6×10^{-5}, they are expected to form a film ~12 nm thick on the surface of the electrode which is approximately a monolayer of particles.

Once assembled into a two-dimensional film, the movement of particles can be described by the convection-diffusion equation,[3]

$$\frac{\partial n(r,t)}{\partial t} + \nabla \cdot [n(\boldsymbol{r},t)\boldsymbol{U}(\boldsymbol{r},t)] = D\nabla^2 n(\boldsymbol{r},t), \tag{S2}$$

where the first term describes the change in particle areal concentration n with time t at a location $\boldsymbol{r}$ on the surface of the electrode, the second term describes the convection of particles due to flow field $\boldsymbol{U}$, and the final term represents the diffusion of the particles with diffusion coefficient D, which is assumed to be constant. The total number of particles is not changing and as a result no source or sink term is included.

After assembly onto one electrode due to electrophoresis, the initial areal concentration n_0 on the positively charged electrode is given by,

$$n_0 = \frac{3\varphi_0 H}{4\pi R^3}, \tag{S3}$$

where φ_0 is the bulk volume fraction and H is the chamber height. In the Cahn-Hilliard analysis, a plane wave perturbation n' is added and the growth or decay of this term will determine the stability of the film. This leads to an expression,

$$n(\mathbf{r}, t) = n_0 + a(t)e^{ikx}, \tag{S4}$$

where $a(t)$ is the amplitude of the wave perturbation, k is the non-dimensional wave vector normalized by R, and x is a direction along the electrode. We assume that initially the perturbation n' is small compared to n_0. Due to this perturbation, the flow field can be separated into $\mathbf{U} = \mathbf{U}_0 + \mathbf{U}'$ where $\mathbf{U}_0$ is due to n_0 and $\mathbf{U}'$ is due n'. However, we assume the initially uniform distribution of particles indicates that $\mathbf{U}_0 = 0$. Thus, Eq. S2 can be linearized to show,

$$\frac{\partial n'}{\partial t} + n_0 \nabla \cdot \mathbf{U}' = D\nabla^2 n'. \tag{S5}$$

By introducing Eq. S4 into Eq. S5 and simplifying, the expression becomes,

$$e^{ikx}a'(t) + n_0 \nabla \cdot \mathbf{U}' = Da(t)\nabla^2 e^{ikx}. \tag{S6}$$

Drawing from the analysis performed by Hardt et al,[4] we define $\mathbf{U}'$ generally using the integral,

$$U' = \frac{-a(t)e^{ikx}i}{4\pi\eta} \int_{-\pi}^{\pi} \int_0^{\infty} \sin(kr\cos\theta) \cos(\theta) \cdot v(r) \, dr d\theta, \tag{S7}$$

where $v(r)$ is the flow velocity as a function of the magnitude of the location r in the x-y plane and θ describes the direction of r. Importantly, there were two flow types present in our system, electroosmotic (EO) and electrohydrodynamic (EHD) flow. The EHD velocity $v_{EHD}(r)$ and EO velocity $v_{EO}(r)$ can be defined as,

$$v_{EHD}(r) = V^2 \gamma_{EHD} f_{EHD}(r) \tag{S8}$$

and

$$v_{EO}(r) = V_{DC} \gamma_{EO} f_{EO}(r), \tag{S9}$$

where the functions $f(r)$ describe the flow at a point r away from a single particle based on the flow profiles in Fig. 4(d) which were replotted from theory described by Ristenpart et al.[5] and the constants γ describe the strength of the flow field with subscripts denoting EHD and EO flow. It is known that EHD flow is proportional to the voltage squared, whereas EO flow scales directly with the applied voltage[5] as described in Eqs. S8 and S9. For each flow, the integral in Eq. S7 was solved numerically as a function of k. Thus, Eq. S7 can be expressed as,

$$U'(k) = \frac{-a(t)e^{ikx}i}{4\pi\eta} (V^2 \gamma_{EHD} W_{EHD}(k) + V_{DC} \gamma_{EO} W_{EO}(k)), \tag{S10}$$

where $W_{EHD}(k)$ and $W_{EO}(k)$ are the result of the double integral described by Eq. S7 for f_{EHD} and f_{EO}, respectively. The plot of $W(k)/k$ in Fig. S1 for EHD shows that at low k (or high wavelength λ) repulsion between particles is expected.

To apply this understanding to our data, Eq. S10 was introduced into Eq. S6 and simplified,

$$a'(t) = a(t)\left(-Dk^2 + \frac{kn_0}{4\pi\eta} (V^2 \gamma_{EHD} W_{EHD}(k) + V_{DC} \gamma_{EO} W_{EO}(k))\right), \tag{S11}$$

which describes the evolution of the amplitude over time. When the term multiplied by $a(t)$ is positive, the perturbation grows, leading to spinodal decomposition. Thus, Eq. S11, can be used to compute a critical voltage V^* at which an instability will occur which is found to be,

$$V^* = \sqrt{\frac{4\pi\eta Dk}{n_0 \gamma_{EHD} W_{EHD}(k)} - \frac{\gamma_{EO} W_{EO}(k) V_{DC}}{\gamma_{EHD} W_{EHD}(k)}}. \tag{S12}$$
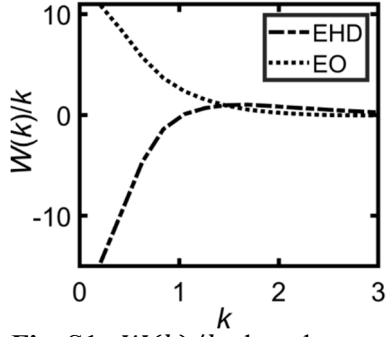
Fig S1. $W(k)/k$ plotted versus wavenumber k for both EHD and EO flows.

Using the Stokes-Einstein equation for D,[6]

$$D = \frac{k_B T}{6\pi\eta R},\qquad(S13)$$

where k_B is Boltzmann's constant and T is temperature, Eq. S12 can be simplified to,

$$V^* = \sqrt{\frac{2k_B T k}{3Rn_0 \gamma_{EHD} W_{EHD}(k)} - \frac{\gamma_{EO} W_{EO}(k) V_{DC}}{\gamma_{EHD} W_{EHD}(k)}}.\qquad(S14)$$

Importantly, Eq. S14 shows that V^* is inversely related to n_0, which implies that as the volume fraction increases, the necessary voltage to observe the cellular phase will decrease. Additionally, V^* must be expanded into its AC and DC components,

$$V^* = V_{AC}^* + bV_{DC},\qquad(S15)$$

where the dimensionless constant b allows V_{AC} and V_{DC} to contribute to EHD with intensities reflecting the different complex conductivities at DC and high frequencies.[5] In our experiments, the critical AC voltage V_{AC}^* at which the cellular phase was observed was determined by fitting the experimental data to a sigmoid as seen in Fig. 3(a),

$$\frac{N}{N_{max}} = a_1 + \frac{a_2}{1+e^{a_3(V_{AC}-V_{AC}^*)}},\qquad(S16)$$

where N is the number of cells, N_{max} is the maximum number of cells observed in that experiment, and a_1, a_2, and a_3 are additional fitting parameters. Incorporating Eq. S15 and S3 into Eq. S14 yields,

$$V_{AC}^* = \sqrt{\frac{8\pi k k_B T R^2}{9H\varphi_0 \gamma_{EHD} W_{EHD}(k)} - \frac{\gamma_{EO} W_{EO}(k) V_{DC}}{\gamma_{EHD} W_{EHD}(k)}} - bV_{DC},\qquad(S17)$$

which was simplified to the functional form used to fit the data in Fig. 3(b),

$$V_{AC}^* = \sqrt{\frac{1}{\beta_{EHD}\varphi_0} - \frac{\beta_{EO} V_{DC}}{\beta_{EHD}}} - bV_{DC}.\qquad(S18)$$

where b, β_{EHD}, and β_{EO} are fitting parameters. Equation S18 captures the behavior in our experimental determination of V_{AC}^* shown in Fig. 3(b) and confirms that as V_{AC}^* increases, φ_0 and V_{DC} decrease.

II. Supplementary Tables and Figures

TABLE S1. Summary of experimental conditions and materials used for previous studies of the cellular phase and this current work.

| Paper	Particle type	Particle diameter	Particle volume fraction	Medium	Field strength
Trau – 1995[7]	Barium titanate	100 nm	0.025 vol%	Castor oil	DC: 0.05 V/μm
Sapozhnikov – 2003[8]	Bronze spheres	120 (& 40) μm	3 vol%	Ethanol toluene mixture	DC: 0.66 V/μm
Kumar – 2005[9]	poly-alpha olefin spheres	45 to 87 μm	0.5 – 10 vol%	Corn oil	AC: 0.1 to 3 kHz, 1.6 – 5 V/μm
Agarwal – 2009[10]	Silica	800 nm	0.07 – 4 vol%	Water + dimethyl sulfoxide mixture	AC: 1 MHz, 1 V/μm
Hardt – 2020[4]	DNA	~350 nm[11] (hydrodynamic diameter)	~0.02 vol%	Dextran and polyethylene glycol	DC: 10-30 V, length across which field is applied is not specified
This work	QDs	17 nm (hydrodynamic diameter)[12]	0.0015 – 0.012 vol%	3.125 mM borate buffer	Typical conditions: DC: 0.01 V/μm AC: 500 kHz, 0.01 V/μm
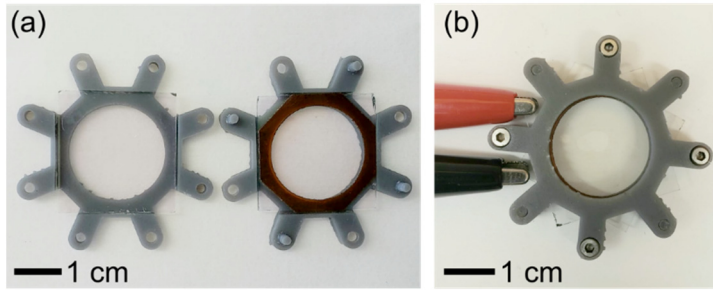
Fig S2. (a) Top and bottom of 3D printed fluid cell frame designed to hold one-inch square indium tin oxide (ITO)-coated glass slides. ITO-glass slides are shown with the polyimide spacer on one slide. Arms were used to align the cell and screw cell together. (b) Fully assembled fluid cell with glass slides, droplet, spacer, screws, and leads.
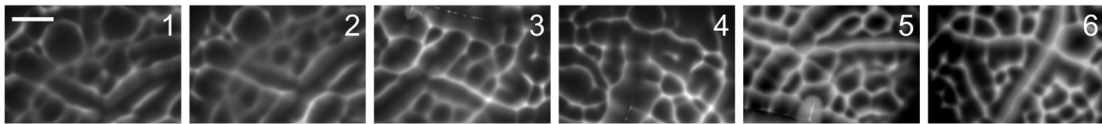

Fig. S3 Fluorescence micrographs of cellular phase formed at $V_{AC} = 2$ V and $V_{DC} = 2.2$ V with QDs at $\varphi = 6 \times 10^{-5}$ throughout six on/off cycles. The scale bar depicts 500 µm. For each image, the field was applied to the fluid cell, it was allowed to stabilize over the course of 4 min. After each image, the field was switched off for 30 min to allow diffusion to homogenize the particle distribution between trials. It was necessary to store the fluid cell in a 100% relative humidity chamber during the diffusion period to prevent evaporation, so the location on the sample imaged in each cycle was not the same.
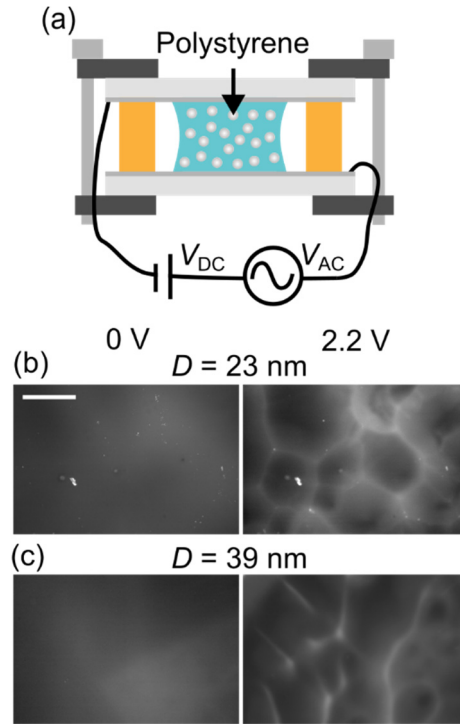
Fig S4. (a) Experimental set-up for fluid cell with polystyrene particles. with a diameter of 26 nm at a volume fraction $\varphi = 9 \times 10^{-5}$. (b) Polystyrene particles with diameter $D = 26$ nm at a volume fraction $\varphi = 9 \times 10^{-5}$. (c) Polystyrene particles with $D = 39$ nm and $\varphi = 1 \times 10^{-3}$. For both (b) and (c), at the left is a fluorescence micrograph of cell when the field was off and at the right is image of cell after applying AC voltage amplitude $V_{AC} = 2$ V with frequency $f = 500$ kHz and turning on DC voltage $V_{DC} = 2.2$ V for 4 min. Scale bar depicts 500 μm and applies to both (b) and (c).
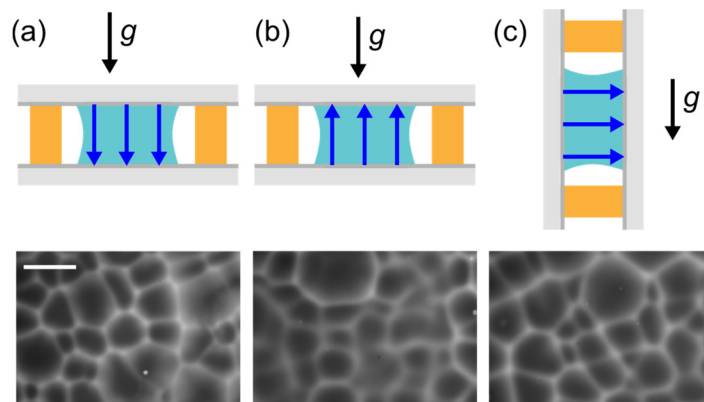

Fig S5. Buoyancy experiments performed with the cell in three orientations relative to gravity g: (a) g and applied electric field E in alignment (b) g and E in opposite directions and (c) g and E perpendicular to one another. Each shows a fluorescence micrograph of the cellular phase at $V_{AC} = 2$ V and $V_{DC} = 2.2$ V with QDs at $\varphi = 6 \times 10^{-5}$ where the QDs accumulate on the positive electrode. The scale bar depicts 500 μm.
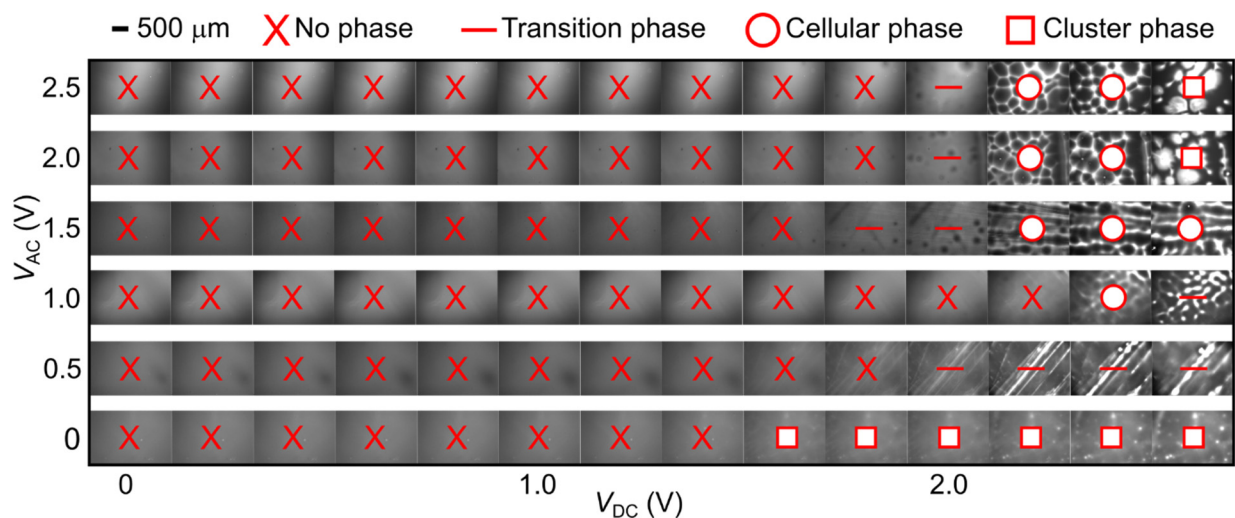
Fig S6. Full set of fluorescence micrographs of assembly experiments of QDs at $\varphi = 6\times10^{-5}$ in which V_{AC} was initially set to a value from 0 V to 2.5 V and then V_{DC} was increased from 0 V to 2.6 V in steps of 0.2 V. After each time V_{DC} was increased, the system was allowed to stabilize for 4 min before images were taken.
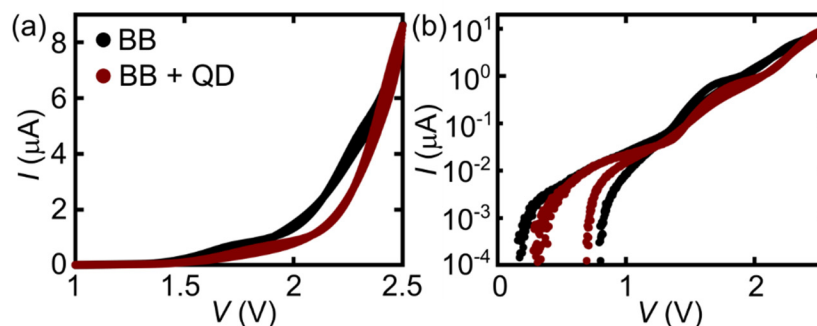

Fig S7. Current I versus voltage V plots from two-electrode cyclic voltammetry electrochemical measurements conducted at a sweep rate of 20 mV/s using the Gamry Reference 600+ Potentiostat/Galvanostat/ZRA on the fluid cell with 3.125 mM borate buffer (BB) solution and QDs in 3.125 mM borate buffer (QD + BB) solution with $\varphi = 6\times10^{-5}$ in (a) linear and (b) log-y scale.
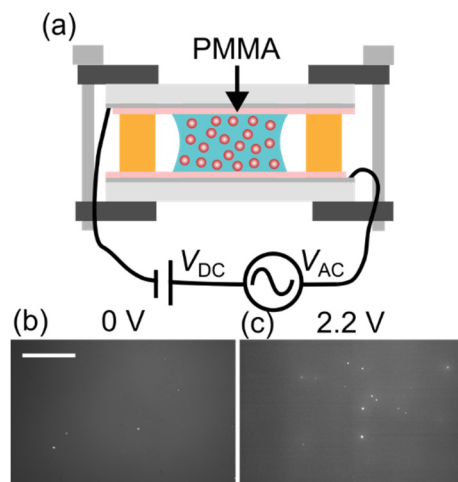
Fig S8. (a) Experimental set-up for fluid cell with polymethylmethacrylate (PMMA) coated ITO glass slides made by spin-coating PMMA (molecular weight = 950 kg/mol, diluted to 6% solids weight) onto both ITO glass slides and then baking them on a hot plate for 2 min at 100℃. (b) Images of top view when field was off with $\varphi = 6\times10^{-5}$. The scale bar depicts 500 µm. (c) Image after applying $V_{AC} = 2$ V and turning on V_{DC} for 4 min.
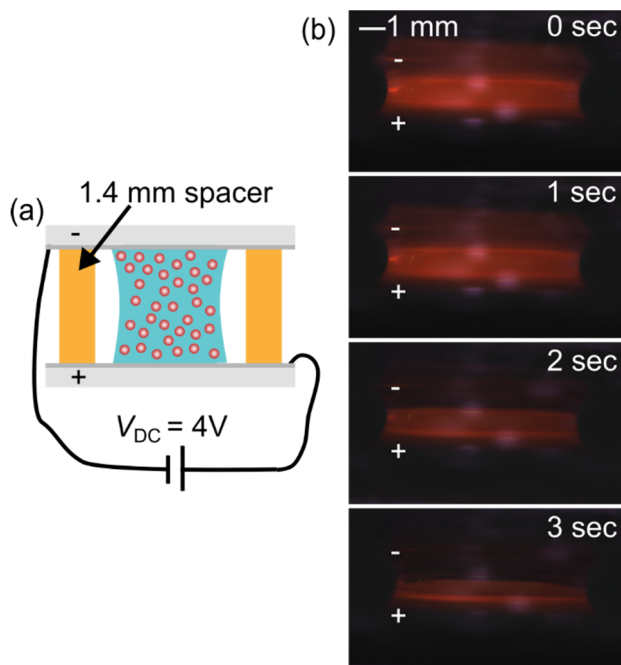

Fig. S9. (a) Schematic of large fluid cell with 1.4 mm spacer which was used in order to image the quantum dot suspension from the side. In this experiment, $V_{DC} = 4$ V in order to maintain a similar DC electric field compared to the typical fluid cell. (b) Images of the quantum dot suspension between the negative and positive electrodes as the particles move to the positive electrode over the course of a few seconds.
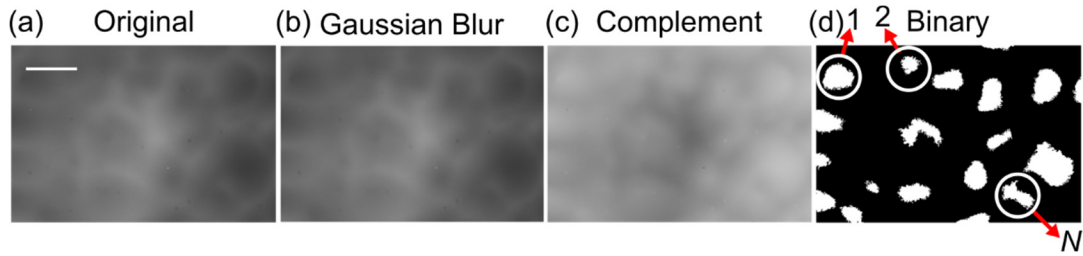
Fig S10. (a) Fluorescence microscopy image taken at 5× magnification of QDs with $\varphi = 3\times10^{-5}$, $V_{DC} = 1.9$ V and $V_{AC} = 4$ V. The scale bar depicts 500 μm. (b) Image after Gaussian blur was applied. (c) Complement of image, white spots indicate voids in the original image. (d) A binary map of the image enabling identification of the number of cells N.
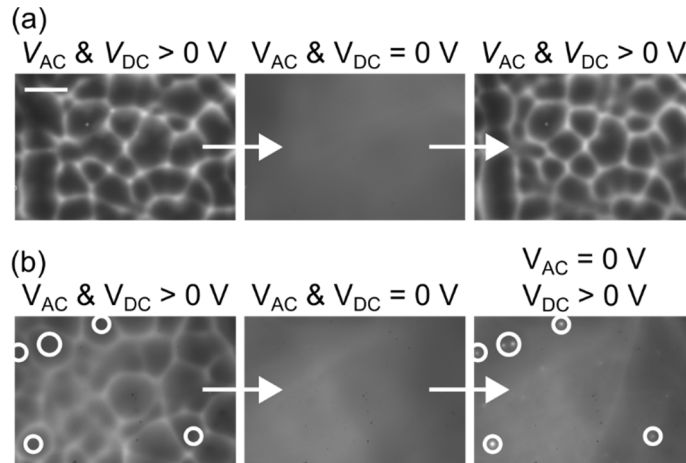

Fig S11. (a) From left to right, micrograph of QDs with $\varphi = 6\times10^{-5}$ when $V_{DC} = 2.2$ V and $V_{AC} = 2$ V after equilibrating for 4 min, then the field was turned off for 40 min to allow the particles to redistribute, and finally the same voltage was applied for 4 min. Scale bar depicts 500 μm and applies to both (a) and (b). (b) From left to right, micrograph of QDs at $\varphi = 6\times10^{-5}$ after $V_{DC} = 2.2$ V and $V_{AC} = 3$ V had been applied for 4 min, micrograph taken after 40 min after the field had been turned off, and then a micrograph taken after $V_{DC} = 2.4$ V was subsequently applied for 4 min. The location of bright spots where QD concentration is high are indicated by the white circles, these same spots correspond to the location of voids in the left-most micrograph.

References

1   J. H. Dickerson and A. R. Boccaccini, *Electrophoretic Deposition of Nanomaterials*, Springer, 2011.

2   S. Mahendra, H. Zhu, V. L. Colvin and P. J. Alvarez, *Environmental Science and Technology*, 2008, **42**, 9424–9430.

3   T. Stocker, *Introduction to Climate Modeling*, Springer, 2011.

4   S. Hardt, J. Hartmann, S. Zhao and A. Bandopadhyay, *Physical Review Letters*, 2020, **124**, 64501.

5   W. D. Ristenpart, I. A. Aksay and D. A. Saville, *Langmuir*, 2007, **23**, 4071–4080.

6   S. E. Spagnolie, *Complex Fluids in Biological Systems*, Springer, 2015.

7   M. Trau, S. Sankaran, D. A. Saville and I. A. Aksay, *Langmuir*, 1995, **11**, 4665–4672.

8   M. v. Sapozhnikov, Y. v. Tolmachev, I. S. Aranson and W. K. Kwok, *Physical Review Letters*, 2003, **90**, 4.

9   A. Kumar, B. Khusid, Z. Qiu and A. Acrivos, *Physical Review Letters*, 2005, **95**, 3–6.

10   A. K. Agarwal and A. Yethiraj, *Physical Review Letters*, 2009, **102**, 100–103.

11   B. Wang, D. Sun, C. Zhang, K. Wang and J. Bai, *Analytical Methods*, 2019, **11**, 2778–2784.

12   W. Cao, M. Chern, A. M. Dennis and K. A. Brown, *Nano Letters*, 2019, **19**, 5762–5768.